Research Article | Vol. 8, No. 7 | 1 Jul 2017 | BIOMEDICAL OPTICS EXPRESS 3449
Biomedical Optics EXPRESS

Photoacoustic/ultrasound dual imaging of human thyroid cancers: an initial clinical study

MENG YANG,[1,5] LINGYI ZHAO,[2,5] XUJIN HE,[3] NA SU,[1] CHENYANG ZHAO,[1] HEWEN TANG,[1] TAO HONG,[4] WENBO LI,[1] FANG YANG,[3] LIN LIN,[1] BING ZHANG,[1] RUI ZHANG,[1] YUXIN JIANG,[1,*] AND CHANGHUI LI[2]

[1]*Department of Ultrasonography, Peking Union Medical College Hospital, Chinese Academy of Medical Sciences & Peking Union Medical College, Beijing 100730, China*
[2]*Department of Biomedical Engineering, College of Engineering, Peking University, Beijing, China*
[3]*Shenzhen Mindray Bio-Medical Electronics Co., Ltd., Shenzhen, China*
[4]*Department of Surgery, Peking Union Medical College Hospital, Chinese Academy of Medical Sciences & Peking Union Medical College, Beijing 100730, China*
[5]*These authors contributed equally to this work*
[*]*yuxinjiangxh@163.com*

Abstract: We reported an initial clinical study of *in vivo* human thyroid by a photoacoustic/ultrasound handheld probe. Our dual-modality system is based on a high-end clinical ultrasound machine. Both healthy and cancerous thyroids were imaged non-invasively, and we compared the photoacoustic imaging with color Doppler ultrasound. The results of photoacoustic thyroid imaging could reveal many blood vessels that were not sensitive for Doppler ultrasound. Our study demonstrated that photoacoustic imaging could provide important complementary information for traditional ultrasound thyroid examination, which has a great potential for clinical diagnosis.

OCIS codes: (110.5120) Photoacoustic imaging; (170.1610) Clinical applications; (170.5120) Photoacoustic imaging.

References and links

1. S. Guth, U. Theune, J. Aberle, A. Galach, and C. M. Bamberger, "Very high prevalence of thyroid nodules detected by high frequency (13MHz) ultrasound examination," N. Engl. J. Med. **351**, 699–706 (2009).
2. H. Gharib, E. Papini, J. R. Garber, D. S. Duick, R. M. Harrell, L. Hegedüs, R. Paschke, R. Valcavi, and P. Vitti; AACE/ACE/AME Task Force on Thyroid Nodules, "American Association Of Clinical Endocrinologists, American College Of Endocrinology, And Associazione Medici Endocrinologi Medical Guidelines for Clinical Practice for the Diagnosis And Management Of Thyroid Nodules–2016 Update," Endocr. Pract. **22**(5), 622–639 (2016).
3. D. S. Cooper, G. M. Doherty, B. R. Haugen, R. T. Kloos, S. L. Lee, S. J. Mandel, E. L. Mazzaferri, B. McIver, S. I. Sherman, and R. M. Tuttle, American Thyroid Association Guidelines Taskforce, "Management guidelines for patients with thyroid nodules and differentiated thyroid cancer," Thyroid **16**(2), 109–142 (2006).
4. L. Hegedüs, "Clinical practice. The thyroid nodule," N. Engl. J. Med. **351**(17), 1764–1771 (2004).
5. B. R. Haugen, E. K. Alexander, K. C. Bible, G. M. Doherty, S. J. Mandel, Y. E. Nikiforov, F. Pacini, G. W. Randolph, A. M. Sawka, M. Schlumberger, K. G. Schuff, S. I. Sherman, J. A. Sosa, D. L. Steward, R. M. Tuttle, and L. Wartofsky, "2015 American Thyroid Association Management Guidelines for Adult Patients with Thyroid Nodules and Differentiated Thyroid Cancer: The American Thyroid Association Guidelines Task Force on Thyroid Nodules and Differentiated Thyroid Cancer," Thyroid **26**(1), 1–133 (2016).
6. S. Zackrisson, S. M. W. Y. van de Ven, and S. S. Gambhir, "Light In and Sound Out: Emerging Translational Strategies for Photoacoustic Imaging," Cancer Res. **74**(4), 979–1004 (2014).
7. P. Beard, "Biomedical photoacoustic imaging," Interface Focus **1**(4), 602–631 (2011).
8. C. Li and L. V. Wang, "Photoacoustic tomography and sensing in biomedicine," Phys. Med. Biol. **54**(19), R59–R97 (2009).
9. L. V. Wang and S. Hu, "Photoacoustic Tomography: In Vivo Imaging from Organelles to Organs," Science **335**(6075), 1458–1462 (2012).
10. A. Garcia-Uribe, T. N. Erpelding, A. Krumholz, H. Ke, K. Maslov, C. Appleton, J. A. Margenthaler, and L. V. Wang, "Dual-Modality Photoacoustic and Ultrasound Imaging System for Noninvasive Sentinel Lymph Node Detection in Patients with Breast Cancer," Sci. Rep. **5**(1), 15748 (2015).

#285574 https://doi.org/10.1364/BOE.8.003449
Journal © 2017 Received 24 Jan 2017; revised 15 May 2017; accepted 19 Jun 2017; published 26 Jun 2017

Biomedical Optics EXPRESS

11. R. A. Kruger, C. M. Kuzmiak, R. B. Lam, D. R. Reinecke, S. P. Del Rio, and D. Steed, "Dedicated 3D photoacoustic breast imaging," Medical Physics **40**, 11 (2013).
12. S. A. Ermilov, T. Khamapirad, A. Conjusteau, M. H. Leonard, R. Lacewell, K. Mehta, T. Miller, and A. A. Oraevsky, "Laser optoacoustic imaging system for detection of breast cancer," J. Biomed. Opt. **14**(2), 024007 (2009).
13. M. Heijblom, D. Piras, W. Xia, J. C. G. van Hespen, J. M. Klaase, F. M. van den Engh, T. G. van Leeuwen, W. Steenbergen, and S. Manohar, "Visualizing breast cancer using the Twente photoacoustic mammoscope: what do we learn from twelve new patient measurements?" Opt. Express **20**(11), 11582–11597 (2012).
14. C. P. Favazza, L. A. Cornelius, and L. V. Wang, "In vivo functional photoacoustic microscopy of cutaneous microvasculature in human skin," J. Biomed. Opt. **16**(2), 026004 (2011).
15. L. Vionnet, J. Gateau, M. Schwarz, A. Buehler, V. Ermolayev, and V. Ntziachristos, "24MHz Scanner for Optoacoustic Imaging of Skin and Burn," Medical Imaging, IEEE Transactions on **PP**, 1 (2013).
16. H. S. Salehi, H. Li, A. Merkulov, P. D. Kumavor, H. Vavadi, M. Sanders, A. Kueck, M. A. Brewer, and Q. Zhu, "Coregistered photoacoustic and ultrasound imaging and classification of ovarian cancer: ex vivo and in vivo studies," J. Biomed. Opt. **21**(4), 046006 (2016).
17. A. Dima and V. Ntziachristos, "In-vivo handheld optoacoustic tomography of the human thyroid," Photoacoustics **4**(2), 65–69 (2016).
18. A. Garcia-Uribe, T. N. Erpelding, A. Krumholz, H. Ke, K. Maslov, C. Appleton, J. A. Margenthaler, and L. V. Wang, "Dual-Modality Photoacoustic and Ultrasound Imaging System for Noninvasive Sentinel Lymph Node Detection in Patients with Breast Cancer," Sci. Rep. **5**(1), 15748 (2015).
19. J. Zalev, B. Clingman, D. Herzog, T. Miller, M. Ulissey, A. T. Stavros, A. Oraevsky, P. Lavin, K. Kist, N. C. Dornbluth, and P. Otto, "Opto-acoustic image fusion technology for diagnostic breast imaging in a feasibility study," in 2015), 941909.
20. J. J. Niederhauser, M. Jaeger, R. Lemor, P. Weber, and M. Frenz, "Combined ultrasound and optoacoustic system for real-time high-contrast vascular imaging in vivo," IEEE Trans. Med. Imaging **24**(4), 436–440 (2005).
21. M. P. Fronheiser, S. A. Ermilov, H. P. Brecht, A. Conjusteau, R. Su, K. Mehta, and A. A. Oraevsky, "Real-time optoacoustic monitoring and three-dimensional mapping of a human arm vasculature," J. Biomed. Opt. **15**(2), 021305 (2010).
22. ANSI, "American National Standard for Safe Use of Lasers," in *Z136.1–2000,* A. N. S. Institute, ed. (ANSI Standard, NY, 2007).
23. Y. Xu, L. V. Wang, G. Ambartsoumian, and P. Kuchment, "Reconstructions in limited-view thermoacoustic tomography," Med. Phys. **31**(4), 724–733 (2004).

1. Introduction

Thyroid is an important organ that primarily influences the metabolic rate and protein synthesis. The prevalence of thyroid nodules is more than 60% [1, 2]. The malignant cases of all the discovered thyroid nodules were about 10%, mainly composed of differentiated thyroid cancer, including papillary thyroid cancer and follicular cancer [3]. The key of the treatment of thyroid nodules highly relies on early detection of thyroid cancer with high accuracy [4].

According to the American Thyroid Association (ATA) guidelines in 2006 [5], ultrasound (US) is recommended as a routine examination of thyroid for all patients with thyroid lesions, as well as healthy people. However, conventional color Doppler ultrasound has limited capacity in discriminating untypical benign and malignant nodules. In recent years, several emerging ultrasound imaging technologies, such as elastography and contrast-enhanced ultrasound (CEUS), have been applied for the clinical evaluation of the thyroid nodule. However, these new imaging techniques have limitations as well. Elastography can only evaluate the stiffness of thyroid nodule semi-quantitatively, and CEUS is rather invasive for the intravenous injection of contrast agent. Therefore, a noninvasive functional imaging modality, with the ability of evaluating the morphological, structural and vascular information simultaneously, will be beneficial to the early diagnosis and clinical management of thyroid cancer.

Photoacoustic (PA) imaging (PAI) is a novel state of the art hybrid imaging modality, which relies on sensitive tissue optical properties, but breaks through the barrier in the imaging depth of high-resolution optical method in living tissue [6–8]. Besides structural imaging, PAI can also provide important functional information, such as the oxygen saturation. Over the past decade, PAI has gained substantial progresses in both technology development and implementations [9]. Besides animal studies, many clinical PAI studies

Biomedical Optics EXPRESS

have been going on worldwide, including breast cancer [10–13], skin diseases [14, 15], ovarian cancer [16], and thyroid [17]. Among those translational studies, integrating PAI with the traditional ultrasound handheld linear probe is always very attractive [16, 18–21]. Not only because the physicians are used to this probe, but also because it has the great potential for PA/US dual modality imaging.

In this study, we developed a dual-modality PA/US system based on a high-end clinical US machine, and performed initial clinical study of in vivo human thyroid, including both healthy and cancerous nodules. We compared PAI with the color Doppler ultrasound image, and our results demonstrated PAI could provide important complementary information for thyroid ultrasound examination.

2. Methods and material

2.1 System setup

Figure 1 shows the system setup, which was based on a modified commercial clinical US system (Resona7, Mindray Bio-Medical Electronics Co., Ltd., China). This high-end US machine is capable to perform parallel data acquisition required by PAI. Besides preserving all US imaging functions, this machine was able to work on receiving-only mode when performing PAI. In this study, we used a clinical linear probe centered at 5.8 MHz and with 192 elements (L9-3U, Mindray Bio-Medical Electronics Co., Ltd., China). The laser source for PAI was a Q-switched Nd:YAG laser (LS-2137/2, LOTIS TII, Minsk, Belarus), which generates 1064-nm laser pulses at 10Hz. A one-two bifurcate optical fiber bundle (made by Nanjing Chunhui Science and technology Industrial Co. Ltd., Nanjing, China) was used to deliver the laser. At this wavelength, hemoglobin in blood serves as the primary optical absorber for PAI.

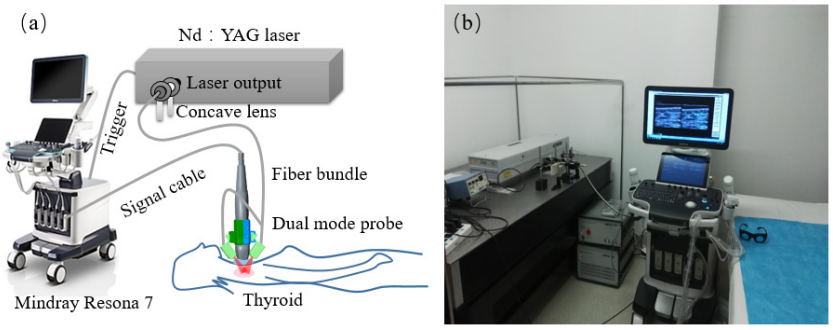

Fig. 1. PA/US imaging system. (a) Schematic. (b) Photograph of the prototype system.

A custom-made holder mounted two bundle terminals on the two sides of the probe, as shown in Fig. 2. To avoid light reaching probe surface that could generate unwanted PA signals, a thin film made of silica gel mixed with TiO_2 particles covered the front surface of the probe. In addition, a 7 mm-thick transparent soft gel pad was placed between the tissue surface and the probe. This pad provided a gap that can allow light shining on the interested area just under the probe without sacrificing US imaging. The area of illumination on the skin was measured to be 10 cm^2, and the optical fluence on the skin surface was 5.5mJ/cm^2, well below the ANSI recommended maximum permissible exposure (MPE) of 100 mJ/cm^2 for this wavelength [22].

Biomedical Optics EXPRESS

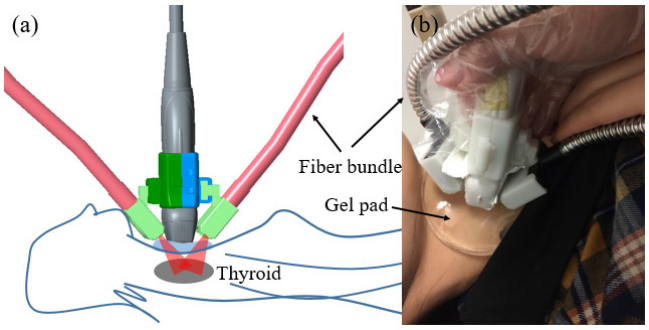

Fig. 2. Dual-modality handheld probe. (a) Schematic. (b) Photograph.

The laser was triggered by the data acquisition system. To guarantee PAI and US to image the same area simultaneously, which is crucial for accurate image co-registration, the US machine triggered the laser to start PAI data acquisition 500 μs after last US imaging frame. The total dual-modality acquisition time was only one second. After data acquisition, PA imaging results were reconstructed off line with the delay and sum algorithm, and each PAI result had been averaged over five frames. Then, gray scale US B-san and PAI fusion image can be constructed.

The PAI image was reconstructed based on the delay&sum algorithm. A band-pass filtering centered at 5.5MHz with bandwidth of 3.5MHz was used on raw PA signals before image reconstruction.

2.2 Phantom study

To validate the performance of the system and the reconstruction algorithm, we did phantom experiments as shown in Fig. 3. A carbon rod with 3-cm long and 0.5-mm in diameter was immersed into a solution made of water and intralipid (1%). We set the rod at different orientation angles and different depths, and fused the reconstructed PAI results with US results. According to all results, the shape and position of the reconstructed PAI results were in good consistent with their US counterparts, which demonstrated that our system can reliably reconstructed the location of the target. In the top row of Fig. 3, the rod was within the imaging plane with different orientation angles: ~30°, 15°, and 0°. The results in Fig. 3(a-c) showed that PA signal decreases with the increase in the orientation angle. It is because that the propagation direction of the generated PA wave from a straight rod primarily is perpendicular to the rod surface, so the incident angle arriving on the probe surface is different for these three angles. However, due to the directivity of the probe, sensitivity will decrease as the relative angle between the incident wave and the norm of the probe becomes larger. Similar results exist when the rod was in a plane perpendicular to the imaging plane. In the second row, Fig. 3(d)-3(f) showed the results at different depths. It is obviously the reconstructed value decreases with depth, primarily due to the attenuation of the optical fluence. All PAI images were plotted in a linear scale, and we used a threshold of 8% of the maximum pixel value. In general, a finite-length handheld US probe has all limitations due to the limited-view, as discussed in detail by Xu [23]. However, since the thyroid node lies relative shallow (~2 cm from the probe), the artifact caused by limited-view is not significant. The signal decrease caused by light fluence attenuation plays a more important role to affect the imaging.

Biomedical Optics EXPRESS

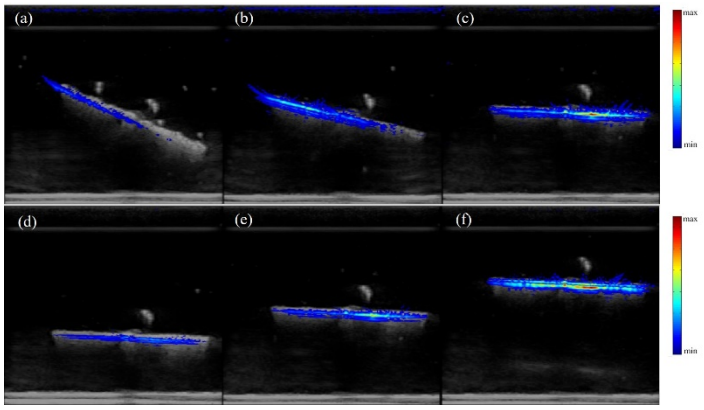

Fig. 3. Dual-modality imaging results of a carbon rod hanged in intralipid solution with different orientation angles (a-c), and different depths (d-f). US results are in gray, and PAI results are in color.

2.3 Patient enrollment

Patients were enrolled consecutively from the outpatients and inpatients of surgery department at Peking Union Medical College Hospital (PUMCH) from Dec. 15th 2016 to Jan. 5th 2017. Our patient enrollment criteria is as following: (1) Ultrasound suspicious malignant thyroid nodules with indication for fine needle aspiration biopsy (FNAB); (2) FNAB and histology proved malignant thyroid nodules. Of all the 10 patients, 5 patients had FNAB. The enrollment of the research is approved by the institutional ethics committee of PUMCH. All the patients have signed the informed consent before performing the examinations.

2.4 PA/US dual mode examination and image processing

All the patients underwent ultrasound examinations including both gray scale and color Doppler flow imaging ultrasound (CDFI) to evaluate the morphological and vascular information of the thyroid nodules, including the margin, position, intranodular structure and the blood flow patterns, etc. PA/US dual imaging was performed right after CDFI. All the examination procedures were approved by the institutional ethics committee of PUMCH.

In the following human study, the reconstructed PA values could have a large dynamic range (~30dB). In order to show PAI more clearly, the reconstructed pixel value of each image was normalized to that image's maximum value, and the final PA image was plotted in log scale. We set the thresholding to be ~10% (−20dB) of the maximum reconstructed PAI value in the fused PA/US image.

Before thyroid imaging, we also imaged the cutaneous vein in the forearm of a healthy adult. We imaged the vessel with the probe parallel to and perpendicular to the vein, respectively, as shown in the top and bottom row of Fig. 4. For comparison, CDFI results were also presented. Due to the very limited penetration of light into blood at this wavelength (~0.2 cm), only boundary of the large vein were successfully reconstructed in PAI images. In addition, due to tissue attenuation and strong blood absorption in vein itself, the upper wall of the vein has a much larger PA value than the bottom wall of the vein, while CDFI does not has this artifact. In addition, due the limited acquisition angle [23], the two side walls of the vein (Fig. 4(f)) in PAI are missing.

Biomedical Optics EXPRESS

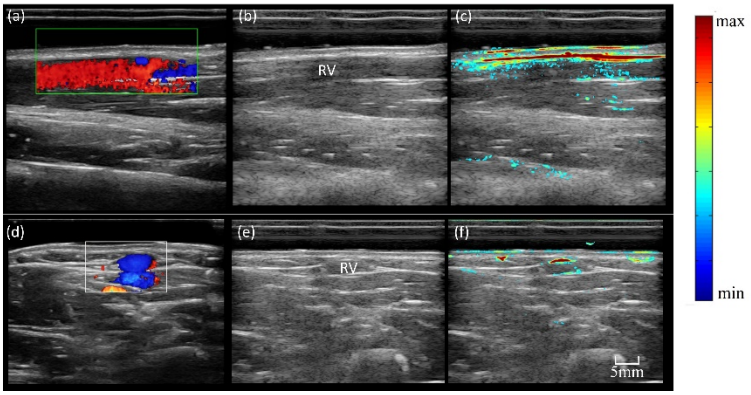

Fig. 4. Imaging results of human forearm cutaneous vein with longitude section and transverse sections. (a) CDFI result with longitude section; (b) gray scale US B-scan with longitude section; (c) PA/US imaging with longitude section; (d) CDFI result with transverse section; (e) gray scale US B-scan with transverse section; (f) PA/US imaging with transverse section;

3. Initial clinical study results

In this initial clinical study, PA/US dual modality imaging was performed in 13 cases, including 3 healthy volunteers with normal thyroid, and 10 patients with suspicious malignant thyroid nodules. The 3 volunteers in our study included 2 female and 1 male, age ranging from 31 to 52years. Ten patients with thyroid nodules were enrolled consecutively from the outpatients and inpatients of surgery department at Peking Union Medical College Hospital (PUMCH) from Dec. 15th 2016 to Jan. 5th 2017. All of the 10 patients with thyroid nodules performed thyroidectomy and pathology confirmed the diagnosis of thyroid cancer, five of them were referred to surgery from FNAB results. There were totally 3 male and 7 female, the median age was 47 years (21-62years).

In the following, one normal and three cancer study results are presented. The CDFI and the PA/US dual imaging information of each case were compared. After presenting PA/US images, Table 1 provides more information of all ten patients, including the age, lesion depth and size, and the histological diagnosis results (some cases include immunohistochemical evaluation (CD34, VEGF, Ki67, etc.)).

Figure 5 showed imaging results for a healthy normal right thyroid, including CDFI (Fig. 5(a)), gray-scale B-scan (Fig. 5(b)), and PA/US (Fig. 5(c)), respectively. Typical anatomical structures were marked in the B-scan result. CDFI (in the white-line box) showed sporadic blood flow in thyroid, while PAI showed abundant PA signals, indicating many more vasculature in the thyroid parenchyma. However, the muscle covering the carotid artery (CA) would attenuate much of the light, which likely caused low PA signal from CA.

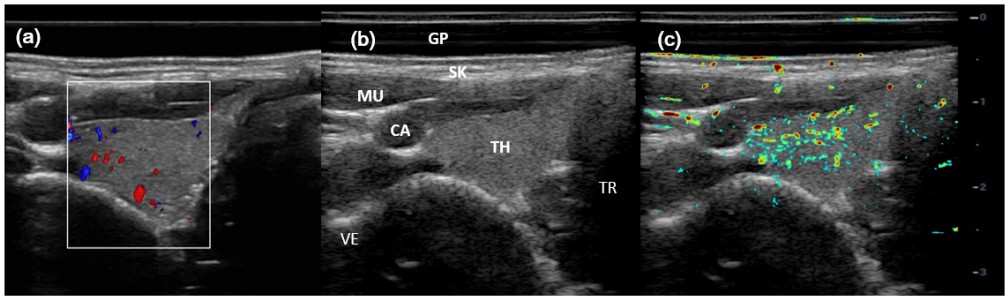

Fig. 5. Imaging results for a healthy right thyroid. (a) CDFI result; (b) gray scale US B-scan; and (c) PA/US imaging result. GP (gel pad), SK (skin), MU (muscle), CA (carotid), TH (thyroid), TR (trachea), VE (vertebrae).

Biomedical Optics EXPRESS

Then, three thyroid cancer imaging results were presented in the following. Figure 6 shows results for case No. 8 in Table 1, which is a left lobe papillary thyroid cancer (PTC, Follicular variation) with the largest diameter of 9 mm. The center of the lesion lies about 1 cm under the skin. Both CDFI and PAI imaging clearly showed the peripheral and intra-nodular vessels. In addition, two highly suspected feeding vessels running under the thyroid subcapsule are better delineated in PA/US imaging (white dashed arrows). The pathological result of this case was right lobe PTC, classical type and 9mm in diameter. The anterior capsular of thyroid and the peripheral muscle was infiltrated by the tumor. H&E and immunohistochemical evaluation was also performed, strong CD34 staining was shown (++) in the thyroid anterior capsular area, which could be taken as the histological proof of vascular existence. VEGF + , and Ki67 1% were also detected in and around the tumor area.

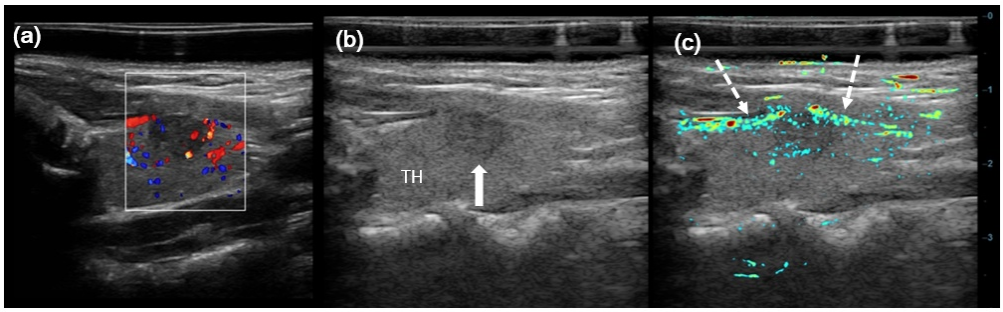

Fig. 6. Imaging results for a left lobe papillary thyroid cancer (PTC, Follicular variation) with the largest diameter of 9 mm. (a) CDFI result; (b) gray scale US B-scan; and (c) PA/US imaging result. Solid white arrow indicates left lobe PTC, and dashed white arrows indicate suspected feeding vessels.

Figure 7 shows results for case No. 9 in Table 1, which is a right lobe papillary thyroid cancer (PTC, Follicular variation) with the largest diameter of 13 mm. The center of the lesion lies about 1.5 cm under the skin. CDFI showed a hyper vascular PTC in the middle of right thyroid, with little blood signal in the surrounding thyroid parenchyma. PA/US result displayed more PA signals in the right lobe PTC and its surrounding thyroid parenchyma.

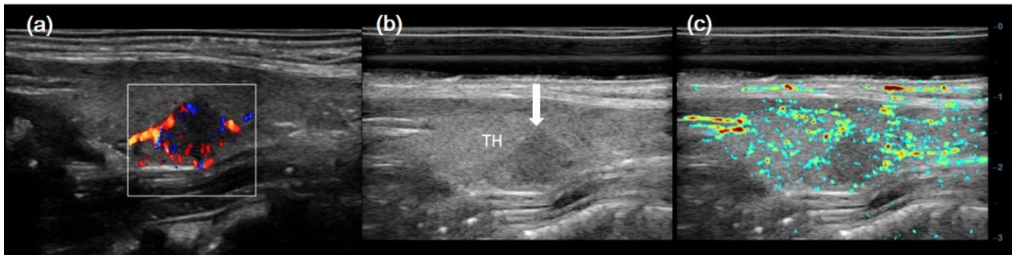

Fig. 7. Imaging results for a right lobe PTC with the largest diameter of 13 mm. (a) CDFI result; (b) gray scale US B-scan; and (c) PA/US imaging result. White arrow indicates right lobe PTC.

Figure 8 shows results for case No. 6 in Table 1, which is another left lobe PTC with the largest diameter of only 3 mm, which is much smaller than the one in Fig. 7. The center of the lesion lies about 1.0 cm under the skin. CDFI showed little blood signals in the left lobe PTC and surrounding thyroid parenchyma. While PA/US imaging displayed more PA signals in left lobe PTC and surrounding thyroid parenchyma than in CDFI.

Biomedical Optics EXPRESS

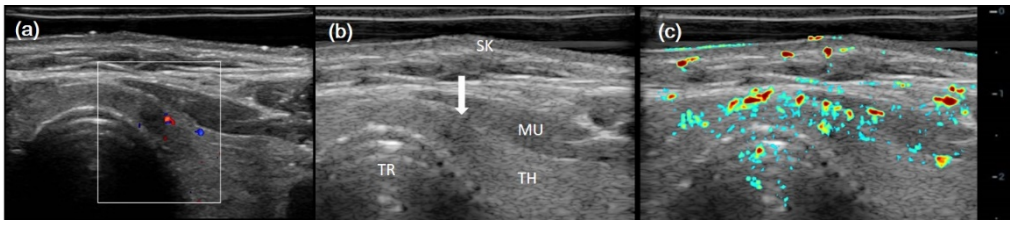

Fig. 8. Imaging results for a left lobe papillary thyroid cancer (PTC, Follicular variation) with the largest diameter of 3 mm. (a) CDFI result; (b) gray scale US B-scan; and (c) PA/US imaging result. White arrow indicates the left lobe PTC.

Table 1. The clinical information, comparison between PAI and US, and histology results

Case No.	Sex	Age	Lesion Depth* (cm)	Size (mm)	PA vs CDFI	Histological diagnosis
1	F	51	1.5	7	PA showed more signals than CDFI	Left lobe papillary thyroid micro- carcinoma (PTMC), with peri-thyroid tissue invasion
2	F	54	1.3	5	PA showed more intra-nodular signal than CDFI	Left lobe PTMC with follicular variation
3	F	52	1.8	5	Due to depth limitation, PA only showed more signals in upper-half of the tumor than CDFI	Left lobe PTMC
4	F	55	1.5	5	PA showed more intra-nodular signal than CDFI	Left lobe PTMC
5	F	62	1.2	7	PA showed similar vascular information with CDFI	Right lobe PTMC
6	M	39	1.3	3	PA showed more peri-nodular signal than CDFI	Left lobe PTMC
7	F	38	1.5	11	PA showed similar vascular information with CDFI	Left lobe PTC with large area of intra- tumor necrosis
8	F	23	1.3	9	PA showed more signal in tumor and anterior thyroid capsular	Right lobe PTC, with invasion of anterior thyroid capsular and peripheral muscles. Ki67: 1%, VEGF + CD34: + +
9	F	37	1.5	13	PA showed more signals than CDFI	Right lobe PTC, with invasion to thyroid capsular and peripheral tissues. CD34 + + + Ki67 2%, VEGF +
10	M	43	Left lobe: 2.5	4	PA showed similar vascular information with CDFI	Left and right lobe PTMC. Ki67 5%, VEGF + , Calectin-3 + , CydinD1 + , CD34 + +
			Right lobe: 3.5	7	CDFI showed more vascular information	

*From the gel surface to the central of lesion.

4. Discussion

To the best of our knowledge, it is the first time to study in vivo human thyroid of both healthy and cancerous cases using a PA/US system. Our PA/US dual modality imaging system showed high quality gray scale ultrasonic and dual-modality fusion images. According

Biomedical Optics EXPRESS

to our results, PAI proved the ability to image both the peripheral and intra-nodular vessels of human thyroid. In addition, that the PA/US result in Fig. 8 showed signal coming from a micro-carcinomas less than 5 millimeters add confidence on the sensitivity of this dual modality imaging technique for diagnosis of small lesions.

Significant differences exist between PAI and CDFI. This is primarily due to the distinct mechanism in these two techniques: CDFI detects blood flow, which highly depends on the blood flow velocity, size, and the direction, whereas PAI depends on the optical absorption, which is much less sensitive to these factors. More specifically, PAI could provide following important complementary information for CDFI, including:

a) PAI can image small vessels and vessels with slow blood flow speed

b) PAI can provide functional imaging besides speed

Based on optical contrast, PAI can perform functional imaging relied on tissue optical properties. For instance, spectroscopic PAI can measure blood oxygen saturation.

However, our study also showed two limitations in PAI. First, PAI signal highly depends on the light fluence in the very heterogeneous living tissue. Therefore, if the light fluence decreased or even was blocked, substantial weak or no PA signals would generate. For instance, it is obvious that the strength of vessel signals become obviously weak as the depth increases in Figs. 6–8. In a more extreme case as for No. 10, whose lesions are much deeper, the PAI does not provide more information than CDFI due to strongly attenuation in light fluence. Second, artifacts would appear in PAI results due to acoustic reflection on large impedance-mismatched boundaries. For instance, there are PA signals in the trachea region in Fig. 5 and Fig. 8. Besides, CDFI can provide important flow information, which is still very challenging for PAI. Therefore, PAI will not replace any US functions, instead, it provides important complementary information for US imaging.

Our study also showed that it is very beneficial to integrate PAI with a high quality clinical US system. Not only because physicians prefer to use a certified instrument for clinical study, but also the clinical US system can provide important high-quality anatomical and functional images, which are crucial to compare and interpret PAI results. We are also working on upgrading this system to real time PA/US display. Further research on the value of PA/US imaging will be performed in larger sample of thyroid nodule cases.

Although this study demonstrated the PAI could provide other structural information than CDFI, it is still very challenging to provide very valuable diagnosis support. One of the most advantage of PAI is its great potential for functional imaging through spectroscopic PAI. In addition, multi-wavelength spectral PAI would be explored in future, which can provide important physiology parameters, such as the blood oxygen saturation. We believe the functional PAI will have potential to differentiate benign and malignant thyroid nodules. Moreover, the system used in this study is also convenient for wide clinical use for many other diseases, such as the breast cancer.

Funding

International S&T Cooperation Program of China (2015DFA30440); National Natural Science Foundation of China (81301268, 81421004); Beijing Nova Program (Z131107000413063). The National Key Instrumentation Development Project (2013YQ030651)